The Exact Support Recovery of Sparse Signals with Noise via Orthogonal Matching Pursuit

Authors: Rui Wu, Wei Huang, and Di-Rong Chen

Publication: IEEE Sig. Proc. Letters, Apr. 2013
Speaker: J. Oliver

Short summary: This letter derives sufficient conditions for the OMP to recover the support set of a sparse vector from noise corrupted measurements. In particular, the conditions are given in terms of the minimum absolute values of the signal amplitudes. That is, if the minimum values of the non-zero coefficient of the signal satisfy certain bound then OMP guarantees exact support recovery**.**

I. System Model and Background

- Consider a model $\mathbf{y} = A\mathbf{x} + \mathbf{e}$, $\mathbf{y} \in R^m$ 정지 $A \in R^{m \times n}$ with $m \ll n$ and $\mathbf{x}$ is a *K*-sparse signal.
- Let A_i be the i*th* column of A and assume that $\|A_i\|_2 = 1, \quad i = 1, 2, \cdots, n$.
- Let $supp(x) = \{i \mid x_i \neq 0\}$ and $|supp(x)| \leq K$.
- The goal of OMP is to estimate the support of $\mathbf{x}$ iteratively.
- At each iteration, OMP selects a column of A that is most correlated with the current residual. OMP then updates the residual by projecting $\mathbf{y}$ onto a linear space spanned by the selected columns. The algorithm iterates until certain stopping rule is satisfied.

A. The OMP algorithm

Notations: For two sets Γ and Λ, let $\Gamma \setminus \Lambda = \{i \mid i \in \Gamma, i \notin \Lambda\}$ and $\Gamma^c = \{1, 2, \cdots, n\} \setminus \Gamma$. Let A_Γ denotes a sub-matrix whose column indices are elements of the set Γ and $\mathbf{x}_\Gamma$ denotes the elements of $\mathbf{x}$ whose indices are specified by Γ and $A_\Gamma^+ = (A_\Gamma^T A_\Gamma)^{-1} A_\Gamma^T$ represents the pseudo-inverse of A.

1. Initialize: Given A and $\mathbf{y}$, set the initial residual vector $\mathbf{r_0} = \mathbf{y}$ (that is $\mathbf{x}_0 = 0$), the initial index set as empty, $\Omega_0 = \Phi$ and the iteration counter t=1.
2. Find the index $i_t = \min_i |\langle A_i, \mathbf{r}_t \rangle|$ and update the support set estimate $\Omega_t = \Omega_{t-1} \cup i_t$
3. Estimate: $\mathbf{x}_t = A_{\Omega_t}^{+}\mathbf{y}$ and update the residual $\mathbf{r}_t = \mathbf{y} - A_{\Omega_t}\mathbf{x}_t$
4. Halt if some stopping rule is satisfied. Otherwise, set t=t+1 and return to step 2.

Stopping rule design for the OMP depends on noise. In noiseless case, (when $\mathbf{e} = 0$) the stopping rule can simply be $\mathbf{r}_t = 0$. This letter considers two types of bounded noises, namely, l_2 bounded noise, $\|\mathbf{e}\|_2 \le \epsilon_1$ and l_∞ bounded noise, $\|A^*\mathbf{e}\|_\infty \le \epsilon_2$. The stopping rules for these two noises in terms of residuals are $\|\mathbf{r}_t\|_2 \le \epsilon_1$ and $\|A^*\mathbf{r}_t\|_\infty \le \epsilon_2$, respectively. This paper also considers the case when e_i follows $\mathcal{N}(0, \sigma^2)$.

II. RIP AND A FEW ASSOCIATED LEMMAS

Two features of a sensing matrix are often used to analyze and derive the recovery performance guarantee of OMP. One is the Mutual Incoherence Property (MIP) [1] defined as $\mu = \max_{i \neq j} |\langle A_i, A_j \rangle|$. And, the other one is restricted isometry property (RIP).

- A matrix A satisfies RIP of order K with parameter δ_K if it is the smallest constant such that

$$(1-\delta_K)\|x\|_2^2 \le \|Ax\|_2^2 \le (1+\delta_K)\|x\|_2^2 \tag{1}$$

  holds for any K-sparse vector $\mathbf{x}$.
- ***Lemma 1:*** Suppose that a matrix A satisfies RIP of order K. Let Γ be an index set with $|\Gamma| \le K$. Then all singular values of sub-matrix A_Γ, which are denoted by $\sigma_i(A_\Gamma)$, satisfy

$$\sqrt{1-\delta_K} \le \sigma_i(A_\Gamma) \le \sqrt{1+\delta_K} \tag{2}$$

- ***Remark 1:*** For any given matrix $B \in R^{m \times n}$, $\|B^*\|_2 = \|B\|_2$. Let $|\Gamma| \le K$, then

$$\|B_\Gamma^*\|_2 = \|B_\Gamma\|_2 = \max_i \sigma_i(B_\Gamma) \le \sqrt{1+\delta_K} \tag{3}$$

- ***Lemma 2:*** Suppose that a matrix *A* satisfies RIP of order *K*. Let Γ be an index set with $|\Gamma| \leq K$. Then all eigenvalues of matrix $A_\Gamma^* A_\Gamma$, which are denoted by $\sigma_i(A_\Gamma^* A_\Gamma)$, satisfy

$$1-\delta_K \leq \sigma_i(A_\Gamma^* A_\Gamma) \leq 1+\delta_K \tag{4}$$

- ***Lemma 3***: Suppose that a matrix *A* satisfies RIP of order *K*. Let Γ and Λ be two disjoint sets with $|supp(\Gamma) \cup supp(\Lambda)| \leq K$. Then for any vector $\mathbf{x}$ with $supp(\mathbf{x}) \subset \Lambda$, it holds that

$$\| (A_\Gamma^* A\mathbf{x})\|_2 = \| (A_\Gamma^* A_\Lambda \mathbf{x}_\Lambda)\|_2 \leq \delta_K \| \mathbf{x}\|_2 \tag{5}$$

Recovery conditions of OMP algorithm			
MIP		RIP	
Noiseless case	Noisy case	Noiseless case	Noisy case
$\mu < \frac{1}{2K-1}$ [3]	$\|x_{min}\| \geq \frac{2\sigma\sqrt{2(1+\alpha)\log N}}{1-(2K-1)\mu}$ [2]	$\delta_{K+1} < \frac{1}{\sqrt{K}+1}$ [4, 5]	$\mu < \frac{1}{2K-1}$ and $\|x_{min}\| \geq \frac{2\varepsilon_1}{1-(2K-1)\mu}$ [6] $\delta_{K+1} < \frac{1}{\sqrt{K}+3}$ and $\|x_{min}\| > \frac{2(1-\delta_{K+1})\epsilon_1}{(1-\delta_{K+1})^2 - \delta_{K+1}(1+\sqrt{K})}$ [7]

III. EXACT SUPPORT SET RECOVERY OF SPARSE SIGNALS

Condition

Let Ω be an original support set of the signal $\mathbf{x}$. Let $\mathbf{r}_{t-1}$ is the residual at the t*th* iteration, $t = 1, 2 \cdots, K$. The condition for OMP to select a correct index at t*th* iteration is

$$\boxed{\| A_{\Omega^c}^* \mathbf{r}_{t-1}\|_\infty < \| A_\Omega^* \mathbf{r}_{t-1}\|_\infty} \tag{6}$$

A. l_2 bounded noise

Theorem 1: Suppose that $\|\mathbf{e}\|_2 \le \epsilon_1$ and the matrix A satisfies condition $\delta_{K+1} < \frac{1}{\sqrt{K}+1}$. Then OMP with stopping rule $\|\mathbf{r}_t\|_2 \le \epsilon_1$ will exactly recover the support Ω of K-sparse signal $\mathbf{x}$, if the minimum magnitude of nonzero elements of $\mathbf{x}$ satisfies

$$\min_{i\in\Omega} |\mathbf{x}_i| \ge \frac{(\sqrt{1+\delta_{K+1}}+1)\epsilon_1}{1-(\sqrt{K}+1)\delta_{K+1}} \tag{7}$$

Proof

- Suppose that OMP selects only correct indexes at the first t-1 iterations, then $\Omega_{t-1} \subseteq \Omega$ and the support of the solution $\mathbf{x}_{t-1}$ obtained at t-1*th* iteration is $supp(\mathbf{x}_{t-1}) \subseteq \Omega$ and $|supp(\mathbf{x}_{t-1})| \le t-1 \le K$.
- We can write the residual $\mathbf{r}_{t-1}$ as

$$\mathbf{r}_{t-1} = \mathbf{y} - A_{\Omega_{t-1}}\mathbf{x}_{t-1} = A_\Omega(\mathbf{x}-\mathbf{x}_{t-1}) + \mathbf{e} \tag{8}$$

- Our goal is to find the RHS and LHS of the condition $\|A_{\Omega^c}^*\mathbf{r}_{t-1}\|_\infty < \|A_\Omega^*\mathbf{r}_{t-1}\|_\infty$

- Let us start with the LHS, that is, $\|A_{\Omega^c}^*\mathbf{r}_{t-1}\|_\infty$

$$\begin{aligned}\|A_{\Omega^c}^*\mathbf{r}_{t-1}\|_\infty &= \|A_{\Omega^c}^*A_\Omega(\mathbf{x}-\mathbf{x}_{t-1}) + A_{\Omega^c}^*\mathbf{e}\|_\infty \\ &\le \|A_{\Omega^c}^*A_\Omega(\mathbf{x}-\mathbf{x}_{t-1})\|_\infty + \|A_{\Omega^c}^*\mathbf{e}\|_\infty \\ &= \max_{i\in\Omega^c} |\langle A_i, A_\Omega(\mathbf{x}-\mathbf{x}_{t-1})\rangle| + \max_{i\in\Omega^c} |\langle A_i, \mathbf{e}\rangle|\end{aligned} \tag{9}$$

- Now from Lemma 3 it holds for any $i \in \Omega^c$

$$|\langle A_i, A_\Omega(\mathbf{x}-\mathbf{x}_{t-1})\rangle| \le \delta_{K+1}\|(\mathbf{x}-\mathbf{x}_{t-1})\|_2$$

- Also, since $\|\mathbf{e}\| \le \epsilon_1$ *and* $\|A_i\|_2 = 1$, we have

$$|\langle A_i, \mathbf{e}\rangle| \le \|A_i\|_2\|\mathbf{e}\|_2 \le \epsilon_1$$

- Now, the LHS becomes

$$\|A_{\Omega^c}^*\mathbf{r}_{t-1}\|_\infty \le \delta_{K+1}\|(\mathbf{x}-\mathbf{x}_{t-1})\|_2 + \epsilon_1 \tag{10}$$

- Let us find the RHS, that is, $\| A_\Omega^* \mathbf{r}_{t-1} \|_\infty$. Let us recall that the residual $\mathbf{r}_{t-1}$ is orthogonal to the columns of $A_{\Omega_{t-1}}$, that is, $A_{\Omega_{t-1}}^* \mathbf{r}_{t-1} = 0$. Then

$$A_\Omega^* \mathbf{r}_{t-1} = \begin{bmatrix} A_{\Omega \setminus \Omega_{t-1}}^* \\ A_{\Omega_{t-1}}^* \end{bmatrix} \mathbf{r}_{t-1} = \begin{bmatrix} A_{\Omega \setminus \Omega_{t-1}}^* \mathbf{r}_{t-1} \\ \mathbf{0} \end{bmatrix}$$

- Thus, $A_\Omega^* \mathbf{r}_{t-1}$ has only $|\Omega \setminus \Omega_{t-1}| = K - (t-1)$ non-zero elements. By using the relation $\| \mathbf{x} \|_\infty \geq \frac{\| \mathbf{x} \|_2}{\sqrt{n}}$, we have

$$\| A_\Omega^* \mathbf{r}_{t-1} \|_\infty \geq \frac{\| A_\Omega^* \mathbf{r}_{t-1} \|_2}{\sqrt{K-(t-1)}}$$

- Now,

$$\begin{aligned} \| A_\Omega^* \mathbf{r}_{t-1} \|_2 &= \| A_\Omega^* A_\Omega (\mathbf{x} - \mathbf{x}_{t-1}) + A_\Omega^* \mathbf{e} \|_2 \\ &\geq \| A_\Omega^* A_\Omega (\mathbf{x} - \mathbf{x}_{t-1}) \|_2 - \| A_\Omega^* \mathbf{e} \|_2 \end{aligned}$$

- $\| A_\Omega^* A_\Omega (\mathbf{x} - \mathbf{x}_{t-1}) \|_2 \geq (1 - \delta_K) \| (\mathbf{x} - \mathbf{x}_{t-1}) \|_2 \geq (1 - \delta_{K+1}) \| (\mathbf{x} - \mathbf{x}_{t-1}) \|_2$ (Consequence of RIP)
- $\| A_\Omega^* \mathbf{e} \|_2 \leq \| A_\Omega^* \|_2 \| \mathbf{e} \|_2 \leq \sqrt{1+\delta_K} \epsilon_1 \leq \sqrt{1+\delta_{K+1}} \epsilon_1$
- Therefore, the RHS is lower bounded by

$$\| A_\Omega^* \mathbf{r}_{t-1} \|_\infty \geq \frac{(1-\delta_{K+1})}{\sqrt{K-(t-1)}} \| (\mathbf{x} - \mathbf{x}_{t-1}) \|_2 - \frac{\sqrt{1+\delta_{K+1}}}{\sqrt{K-(t-1)}} \epsilon_1 \qquad (11)$$

- $\| (\mathbf{x} - \mathbf{x}_{t-1}) \|_2 \geq \sqrt{K-(t-1)} \min_{i \in \Omega} |\mathbf{x}_i|$ (12)

- Using Eqns. (10), (11), and (12), we can find that for the condition (6) to be satisfied , the following inequality must hold true

$$\min_{i \in \Omega} |\mathbf{x}_i| \geq \frac{(\sqrt{1+\delta_{K+1}} + 1)\epsilon_1}{1 - (\sqrt{K}+1)\delta_{K+1}}$$

which is stated in Theorem 1.

- After all the K indexes in Ω have been identified, we find a new estimator via $\mathbf{x}_K = A^+ \mathbf{y}$. Then, the residual $\mathbf{r}_K$ obeys

$$\| \mathbf{r}_K \|_2 = \| \mathbf{y} - A_\Omega \mathbf{x}_K \|_2 \leq \| \mathbf{y} - A_\Omega \mathbf{x} \|_2 = \| \mathbf{e} \|_2 \leq \epsilon_1$$

- Therefore, OMP stops after *K* iterations during which the stopping rule is satisfied.

B. l_∞ bounded noise:

Theorem 2: Suppose that $\| A^* \mathbf{e} \|_\infty \le \epsilon_2$ and the matrix A satisfies condition $\delta_{K+1} < \frac{1}{\sqrt{K}+1}$. Then OMP with stopping rule $\| A^* \mathbf{r}_t \|_\infty \le \epsilon_2$ will exactly recover the support Ω of K-sparse signal $\mathbf{x}$, if the minimum magnitude of nonzero elements of $\mathbf{x}$ satisfies

$$\min_{i \in \Omega} |\mathbf{x}_i| \ge \frac{(\sqrt{1+\delta_{K+1}}+1)\sqrt{K}\epsilon_2}{1-(\sqrt{K}+1)\delta_{K+1}}$$

C. Gaussian noise case

It is well known that when the noise in the model $\mathbf{y} = A\mathbf{x} + \mathbf{e}$ follows iid Gaussian distribution with zero-mean and variance σ^2, then

$$P\left(\| \mathbf{e} \|_2 \le \sigma \sqrt{m + 2\sqrt{m \log m}} \right) \ge 1 - \frac{1}{m}$$

Theorem 3: Suppose that each element of the noise vector follows Gaussian with zero mean and variance σ^2 and the matrix A satisfies condition $\delta_{K+1} < \frac{1}{\sqrt{K}+1}$. Then, OMP with stopping rule $\| \mathbf{r}_t \|_2 \le \sigma \sqrt{m + 2\sqrt{m \log m}}$ will exactly recover the support Ω of *K*-sparse signal $\mathbf{x}$ with probability at least 1-(1/m), if the minimum magnitude of nonzero elements of $\mathbf{x}$ satisfies

$$\min_{i \in \Omega} |\mathbf{x}_i| \ge \frac{(\sqrt{1+\delta_{K+1}}+1)\sigma\sqrt{m + 2\sqrt{m \log m}}}{1-(\sqrt{K}+1)\delta_{K+1}}$$

Remarks:

- In l_2 bounded noise case, the minimum magnitude of the *K*-sparse signal needs to be in the same order of the noise level.
- In l_∞ bounded noise case, the minimum magnitude needs to be about $\sqrt{K}$ times the noise level

- In the Gaussian case, the minimum magnitude depends on the size "*m*" of the matrix. Thus, *m* must be chosen to satisfy $\delta_{K+1} < \frac{1}{\sqrt{K}+1}$ (for example say $m > K^2$), then the minimum magnitude need to be about *K* times of σ.

Reference

[1] D. Donoho and X. Huo, ``Uncertainty principles and ideal atomic decomposition," IEEE Trans. Info. Theory, vol. 47, no. 7, pp. 2845-2862, 2001.

[2] A. B. Heim, Y. Eldar, and M. Elad, ``Coherence-based performance guarantees for estimating a sparse vector under random noise," IEEE Trans. On Sig. Process. vol. 58, no.10, pp. 5030-5042, Oct. 2010.

[3] J. Tropp, ``Greed is good: Algorithmic results for sparse approximation,"IEEE Trans. Info. Theory, vol. 50, no. 10, pp. 2231-2242, 2004.

[4] Q. Mo and Y. Shen, ``A remark on the restricted isometry property in orthogonal matching pursuit," IEEE Trans. Inf. Theory, vol. 58, no. 6, pp. 3654-3656, 2012.

[5] J. Wang and B. Shim, ``On the recovery limit of sparse signals using orthogonal matching pursuit," IEEE Trans. Signal Process., vol. 60, no. 9, pp. 4973-4976, Sept. 2012.

[6] T. Cai and L. Wang, ``Orthogonal matching pursuit for sparse signal recovery with noise," IEEE Trans. Inf. Theory, vol. 57, no. 7, pp.4680–4688, 2011.

[7] Y. Shen and S. Li, ``Sparse signals recovery from noisy measurements by orthogonal matching pursuit," Arxiv Preprint arXiv: 1105.6177, 2011.

Hierarchical and High-Girth QC LDPC codes

Authors: Yige Wang, Stark C. Draper, Jonathan S. Yedidia
Publication: IEEE T. Info.Theory, July 2013
Speaker: Jeong-Min Ryu

Short summary:

They present **an approach to designing capacity approaching high-girth low-density parity-check (LDPC) codes** that are friendly to hardware implementation, and compatible with some desired input code structure defined using a protograph. The approach is based on a mapping of any class of codes defined using a protograph into a family of hierarchical quasi-cyclic (HQC) LDPC codes. Next, they present **a girth-maximizing algorithm** that optimizes the degrees of freedom within the family of codes to yield a high-girth HQC LDPC code, subject to bounds imposed by the fact that HQC codes are still quasi-cyclic. Finally, they discuss **how certain characteristics of a code protograph will lead to inevitable short cycles** and show that **these short cycles can be eliminated** using a "squashing" procedure that results in a high-girth QC LDPC code.

(The "girth" of a code is the length of the shortest cycle in the code graph)

I. INTRODUCTION

1. The construction of LDPC codes

- Highly random graph construction
- Algebraic construction

1) Highly random graph construction

→ It can produce LDPC codes that closely approach the Shannon capacity

→ **Not easy to implement** in hardware as the irregular connections imply wiring complexity.

2) Algebraic construction

→ In actual implementations, more structured constructions have been strongly preferred

→ Quasi- cyclic LDPC (QC LDPC) codes are a particularly practical and widely used class of structured LDPC codes.

→ In view of the practicality, **they focus in this paper on the design of QC LDPC codes** that have good decoding performance

2. Optimizing the decoding performance

- Water-fall
- Error floor

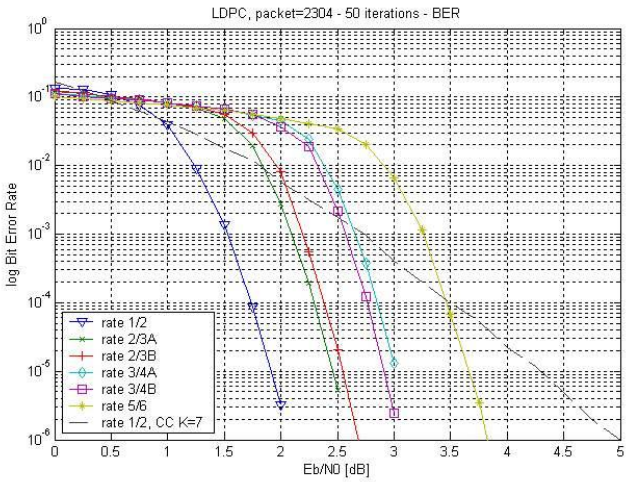

1) Water-fall

→ **"**Water-fall" is a regime where the signal-to-noise (**SNR**) is relatively **low**.

→ The standard way to do that for irregular random constructions is to use "**density-evolution**" or "**EXIT chart**" techniques to obtain the degree distribution that **optimizes the code threshold in the asymptotic limit of long block lengths**

2) Error floor

→ An "error floor" in the performance curve means that **the decoding failure rate does not continue to decrease rapidly as the SNR increases**.

In this paper, they focus on how to take a code structure, such as a particular spatial-coupling structure, that has been designed to perform near the Shannon limit in the waterfall regime, and constructing a QC LDPC code with that structure that also empirically has excellent error floor performance.

II. QC LDPC CODES

- **Review of Standard QC LDPC codes**

QC LDPC codes are defined in terms of **circulant permutation matrices**. Let $I_{i,p}$ denote the circulant permutation matrix, or "cyclic shift matrix," obtained by cyclically left-shifting a $p \times p$ identity matrix by i positions, where $0 \le i \le p-1$; $I_{0,p}$ is thus the $p \times p$ identity matrix. We often suppress the dependence on p, writing I_i instead of $I_{i,p}$. As an example, if $p = 4$, then

$$I_1 = \begin{bmatrix} 0 & 0 & 0 & 1 \\ 1 & 0 & 0 & 0 \\ 0 & 1 & 0 & 0 \\ 0 & 0 & 1 & 0 \end{bmatrix}.$$

An important special case of QC LDPC codes is "weight-I (J, L) regular" QC LDPC code. The parity check matrix of such a code consists of J rows and L columns of $p \times p$ cyclic shift submatrices. The submatrix in the jth row and lth column is $I_{i_{j,l}} = (I_1)^{i_{j,l}}$ and the code has blocklength $N = pL$. They abstractly represent the (j,l)th submatrix as a power of dummy variable x as $x^{i_{j,l}}$.

More generally, a QC LDPC code is represented by a polynomial parity check matrix $H(x)$ whose entries are polynomials in x:

$$H(x)=\begin{bmatrix} h_{1,1}(x) & h_{1,2}(x) & \cdots & h_{1,L}(x) \\ h_{2,1}(x) & h_{2,2}(x) & \cdots & h_{2,L}(x) \\ \vdots & & \ddots & \vdots \\ h_{J,1}(x) & h_{J,2}(x) & \cdots & h_{J,L}(x) \end{bmatrix}$$

where $h_{j,l}(x)=\sum_{s=0}^{p-1} c_s[j,l]x^s$ for $1\le j\le J, 1\le l\le L$, $c_s[j,l]\in\{0,1\}$.

Example 1: Let *C* be a length-9 QC LDPC code described by

$$\mathbf{H}=\left[\begin{array}{ccc|ccc|ccc} 1&0&0&1&0&0&1&0&0\\ 0&1&0&0&1&0&0&1&0\\ 0&0&1&0&0&1&0&0&1\\ \hline 0&0&0&1&0&0&0&1&1\\ 0&0&0&0&1&0&1&0&1\\ 0&0&0&0&0&1&1&1&0 \end{array}\right]$$

For this code, $J=2, L=3$, and $p=3$, and H can equivalently be written as

$$\mathbf{H}=\begin{bmatrix} \mathbf{I}_0 & \mathbf{I}_0 & \mathbf{I}_0 \\ \mathbf{0} & \mathbf{I}_0 & \mathbf{I}_1+\mathbf{I}_2 \end{bmatrix}.$$

The polynomial version of the parity check matrix is

$$\mathbf{H}(x)=\begin{bmatrix} x^0 & x^0 & x^0 \\ 0 & x^0 & x^1+x^2 \end{bmatrix}=\begin{bmatrix} 1 & 1 & 1 \\ 0 & 1 & x^1+x^2 \end{bmatrix}.$$

For the maximum weight *M* among all polynomial entries $h_{j,l}(x)$ in $H(x)$, they call such a code a weight-*M* QC-LDPC code.

The code in Example 1 is a weight-II QC LDPC code.

III. Graphical Representations of QC LDPC Codes

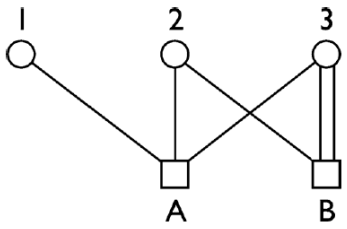

Fig. 1. A simple protograph with three types of variables and two types of checks.

A "**protograph**," as introduced by Thorpe in [30], is a template that can be used to derive a class of Tanner graphs. **Each node in a protograph represents a "type" of node** in a Tanner graph. The nodes will all be duplicated p times in the Tanner graph derived from the protograph.

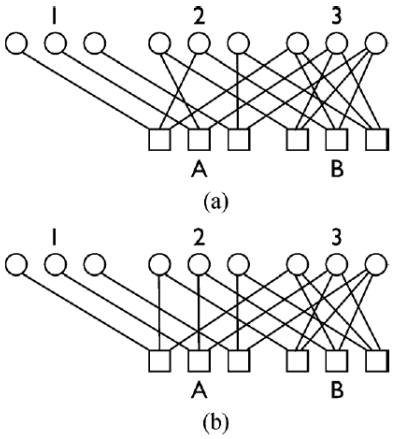

Fig. 2. Two Tanner graphs corresponding to the protograph shown in Fig. 1. The Tanner graph in (a) does not have a quasi-cyclic structure; the one in (b) does, and in fact has the parity check matrix of the QC LDPC code given in Example 1.

Fig. 2 shows two Tanner graphs derived from the protograph of Fig.1, with $p = 3$. Note that there are many possible Tanner graphs that one can construct, which correspond to a particular protograph, and they need not necessarily have a quasi-cyclic structure. The Tanner graph shown in Fig. 2(a) is not quasi- cyclic. But it is always easy to construct a quasi-cyclic version of any protograph.

Protographs can equivalently be described by an **"incidence" matrix**. An incidence matrix has a number of rows equal to the number of types of checks in the protograph and a number of

columns equal to the number of types of variables. Each entry in the incidence matrix tells you how many edges there are connecting a type of check node to a type of variable node in the protograph. For example, the incidence matrix P for the protograph in Fig.1 would be

$$P = \begin{bmatrix} 1 & 1 & 1 \\ 0 & 1 & 2 \end{bmatrix}.$$

- **Lifting procedure** (used to maximizes the girth of the code)

The lifting procedure is simply to replace each entry in the incidence matrix with a polynomial of weight equal to the entry.

For example, the protograph in Fig. 1, which has the incidence matrix P, can be lifted into a QC LDPC code with parity check matrix

$$H(x) = \begin{bmatrix} x^a & x^b & x^c \\ 0 & x^d & x^e + x^f \end{bmatrix},$$

where $a, b, c, d, e,$ and f are integer exponents between 0 and $p-1$, with $e \neq f$. These integer exponents **parameterize an ensemble of QC LDPC codes** all of which are liftings of (and which cover) the original protograph. In our algorithms, **they will optimize over the choice of these exponents to find a lifting that maximizes the girth of the resulting code**.

IV. Cycles in QC LDPC Codes

- How to identify cycles in QC LDPC codes from their parity check matrix
- For weight-I QC LDPC codes → For higher weight QC LDPC codes
- Review of an obstacle in constructing QC LDPC codes with good girth (The higher weight QC LDPC codes with certain characteristics are inevitable to have short cycles)
- HQC LDPC codes overcome the obstacle
- Applying a lifting transformation into HQC codes to obtain high-girth QC codes.

A. Finding Cycles in Weight-I QC LDPC codes

- **Cycle**

A cycle is a path through nodes in the Tanner graph of a code. It alternates between check and variable nodes, and starts and ends at the same node.

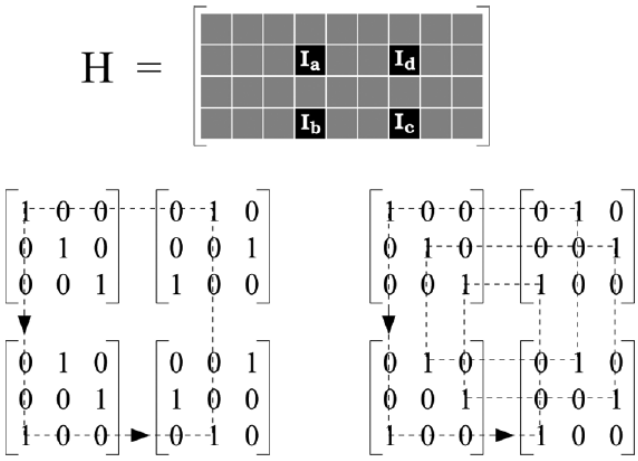

Fig. 3. A parity-check matrix and four 3×3 circulant permutation matrices ($\mathbf{I}_a$, $\mathbf{I}_b$, $\mathbf{I}_c$ and $\mathbf{I}_d$) selected from it. One set of parameters (lower left, $a = 0$, $b = 2$, $c = 1$, $d = 2$) results in a cycle of length four. An alternate set (lower right, $a = 0$, $b = c = d = 2$) results in a cycle of length twelve.

- **Condition of the cycles for weight-I QC LDPC codes**

They specify the conditions on the $\{a,b,c,d\}$ developed in [33] that result in a cycle. **Calculate an alternating sum of the shift indices associated with neighboring permutation matrices along a given path (every odd shift index is subtracted rather than added)**. For example, consider the left-hand path of Fig. 3. The sum is $-a+b-c+d$. Only if the differences sum to zero (mod-p) at the end of the path will the path return to the same variable node in the starting permutation matrix, thereby forming a cycle. For the example of Fig. 3, the condition for a length-four cycle to exist is:

$$(-a+b-c+d) \mod p = 0,$$

which is satisfied for $a=0, b=2, c=1, d=2$, but is not satisfied by $a=0, b=c=d=2$.

B. Finding Cycles in Higher Weight QC LDPC codes

Let us take the matrix $H(x)$ of Exmple 1,

$$H(x)=\begin{bmatrix} x^0 & x^0 & x^0 \\ 0 & x^0 & x^1+x^2 \end{bmatrix}.$$

Now, consider the following ordered series:

$$O=\{(1,2),(2,2),(2,3),(2,3),(2,3),(1,3)\}$$

where each pair (j,l) in O satisfies $1\le j\le J=2$ and $1\le l\le L=3$. This ordered series specifies a sequence of rectilinear moves through $H(x)$.

To specify a candidate cycle through the Tanner graph, we associate a coefficient index *s* with each pair (j,l) in O, such that $c_s[j,l]\neq 0$. They denote this series of coefficient indices by S. **The candidate cycle will be a cycle if the alternating sum of coefficient indices in *S* modulo *p* equals zero**.

In their example, consider the two following choices for the respective (ordered) sets of coefficient indices:

$$S_a=\{0,0,1,2,1,0\}$$
$$S_b=\{0,0,2,1,2,0\}.$$

Each of these choices corresponds to a cycle of length-6 through the Tanner graph of the code. The alternating sums modulo-3 can be verified to be equal to zero. Respectively, these sums are

$$(-0+0-1+2-1+0)\bmod 3=0$$
$$(-0+0-2+1-2+0)\bmod 3=0.$$

C. Invertible Cycles in Higher Weight QC LDPC codes

An important theorem proven by Smarandache and Vontobel [35] states that any weight-III QC LDPC code will inevitably contain cycles of length six. Suppose that, without loss of generality, the polynomial $h_{j,l}(x)$ is weight-III and has the form $x^a + x^b + x^c$. To see that a cycle must exist using thier notation, choose the length-six ordered series

$$O = \{(j,l),(j,l),(j,l),(j,l),(j,l),(j,l)\},$$

and choose $S = \{a,b,c,a,b,c\}$. We find that

$$(-a+b-c+a-b+c) \mod p = 0,$$

for any value of *p*.

One can also prove (see [35, Th. 17] or [27, Example 3.3]) that a parity check matrix of a weight-II QC LDPC code that contains two weight-2 polynomials in the same row or the same column will inevitably have eight-cycles. To see this, suppose the two weight-2 polynomials are in the same row j, but in two different columns $l_1 \neq l_2$. Let $h_{j,l_1} = x^a + x^b$ and $h_{j,l_2} = x^c + x^d$. Consider the length-eight ordered series

$$O = \{(j,l_1),(j,l_1),(j,l_2),(j,l_2),(j,l_1),(j,l_1),(j,l_2),(j,l_2)\}$$

and choose

$$S = \{a,b,c,d,b,a,d,c\}.$$

We again find that

$$(-a+b-c+d-b+a-d+c) \mod p = 0,$$

regardless of the value of *p*.

These inevitable six-cycles and eight-cycles appear to put serious limitations on what protographs can be converted into quasi-cyclic codes with high girth.

V. HQC LDPC CODES

- To solve the problem of invertible short cycles, they introduce HQC LDPC codes.
- An HQC LDPC code is formed from "levels" that each has a quasi-cyclic structure. The structure can be specified in two forms:
  1) Polynomial parity check matrices
  2) Tree structure
- They connect the hierarchical structure to a particular sequence of liftings of a base graph.

A. Parity Check Matrices of HQC LDPC Codes

Example 2: Consider the polynomial parity check matrix specified in (18) with $p=8$. Because the highest weight of any of the polynomial entries is 2, and because there are 12 columns in the matrix, this is a length-96 weight-II QC LDPC code

$$\mathbf{H}(x)=\left[\begin{array}{ccc|ccc|ccc|ccc} x^6 & 0 & x^1+x^7 & 0 & x & 1+x^2 & 0 & 0 & 0 & x^6 & x^3 & 1 \\ x^1+x^7 & x^6 & 0 & 1+x^2 & 0 & x & 0 & 0 & 0 & 1 & x^6 & x^3 \\ 0 & x^1+x^7 & x^6 & x & 1+x^2 & 0 & 0 & 0 & 0 & x^3 & 1 & x^6 \\ \hline 0 & x & 1+x^2 & x^6 & 0 & x^1+x^7 & x^6 & x^3 & 1 & 0 & 0 & 0 \\ 1+x^2 & 0 & x & x^1+x^7 & x^6 & 0 & 1 & x^6 & x^3 & 0 & 0 & 0 \\ x & 1+x^2 & 0 & 0 & x^1+x^7 & x^6 & x^3 & 1 & x^6 & 0 & 0 & 0 \end{array}\right] \tag{18}$$

$$\mathbf{H}(x,y)=\left[\begin{array}{c|c|c|c} x^6+(x+x^7)y & (1+x^2)y+xy^2 & 0 & x^6+y+x^3y^2 \\ \hline (1+x^2)y+xy^2 & x^6+(x+x^7)y & x^6+y+x^3y^2 & 0 \end{array}\right] \tag{19}$$

$$\mathbf{H}(x,y,z)=\left[x^6+(x+x^7)y+((1+x^2)y+xy^2)z \;\middle|\; (x^6+y+x^3y^2)z\right] \tag{20}$$

Each of the three contractions of the parity check matrix of this code into the polynomial parity check matrices represented by (18), (19), and (20), corresponds to a "level" in the hierarchy of this **three-level** HQC LDPC code.

We now present a formal definition of the family of *K*-level HQC LDPC codes which generalizes our example.

Definition 1: An HQC LDPC code with K levels is defined by a $J_{[k]} \times L_{[k]}$ multivariate polynomial parity check matrix $H(\cdot)$ in *K* variables. The entry in the *j*th row and *l*th column of $H(\cdot)$, $1 \le j \le J_{[k]}$, $1 \le l \le L_{[k]}$ is a *K*-variate polynomial $h_{j,l}(\cdot,\cdots,\cdot)$ over the *K* variables $x_{[1]},\ldots,x_{[k]}$. With these definitions, we defined the code by the $J_{[k]} \cdot L_{[k]}$ polynomials

$$h_{j,l}(x_{[1]},\ldots,x_{[K]}) = \sum_{s_K=0}^{p_{[K]}-1} \cdots \sum_{s_1=0}^{p_{[1]}-1} c_{s_1,\ldots,s_K}[j,l] \left(\prod_{k=1}^{K} x_{[k]}^{s_k} \right).$$

Example) We can rewrite the term $h_{1,1}(x,y,z)$ of (20) as

$$\mathbf{H}(x,y,z) = \left[x^6 + (x+x^7)y + ((1+x^2)y + xy^2)z \;\middle|\; (x^6 + y + x^3y^2)z \right] \tag{20}$$

$$\begin{aligned} & h_{1,1}(x_{[1]},x_{[2]},x_{[3]}) \\ &= x_{[1]}^6 + \left(x_{[1]} + x_{[1]}^7\right) x_{[2]} + \left(\left(1 + x_{[1]}^2\right) x_{[2]} + x_{[1]} x_{[2]}^2\right) x_{[3]} \\ &= \sum_{s_3=0}^{1} \sum_{s_2=0}^{2} \sum_{s_1=0}^{7} c_{s_1,s_2,s_3}[1,1] x_{[1]}^{s_1} x_{[2]}^{s_2} x_{[3]}^{s_3}, \end{aligned}$$

where all coefficients $c_{s1,s2,s3}[1,1]$ are zero except for

$$c_{6,0,0}[1,1] = c_{1,1,0}[1,1] = c_{7,1,0}[1,1] = c_{0,1,1}[1,1] = c_{2,1,1}[1,1] = c_{1,2,1}[1,1] = 1.$$

B. Tree Structure of HQC LDPC Codes

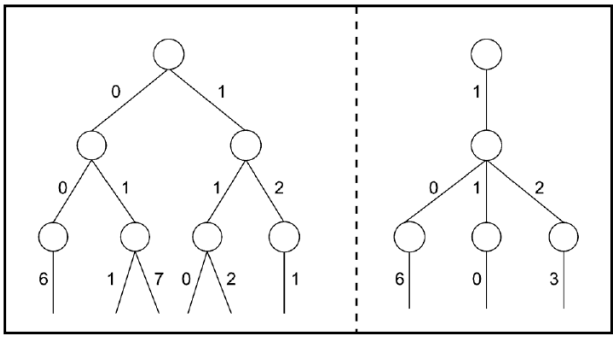

Fig. 4. Example of the tree structure of a family of three-level HQC LDPC codes. The left-hand tree is $\mathbf{T}_{1,1}$, and the right-hand tree is $\mathbf{T}_{1,2}$.

Remained contests

- **Finding cycles in HQC LDPC codes**
- **Inevitable cycles in HQC LDPC codes**

- **Proposing girth maximization using hill climbing**

- **Design of restricted two-level HQC LDPC codes (The additional "restriction" is that the weight of the first(lowest) level must be one)**
  →The restricted two-level HQC LDPC codes can considered weight-I QC LDPC codes
- **Squaring sets of trees to eliminate inevitable cycles**

- **Design of high-girth codes**

Numerical Result

In Figs. 9, 10, and 11, they plot the respective error rate performance of the three codes for the binary symmetric channel (BSC). For purposes of comparison, they plot analogous results for some randomly generated girth-6 QC LDPC codes. These codes have the same length, same rate, and same nonzero positions in the base matrix (i.e., same protograph structure) as the girth-10 and girth-8 codes to which they are compared.

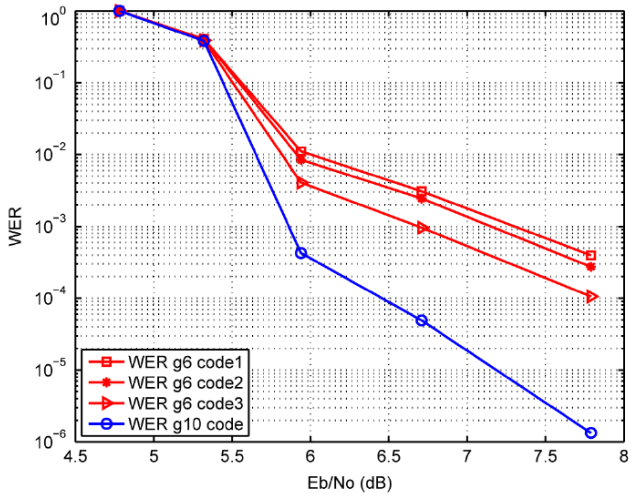

Fig. 9. Word-error rate plots of the Gallager-B algorithm for the rate-0.45, length-8000 girth-6 and girth-10 QC LDPC codes over the BSC.

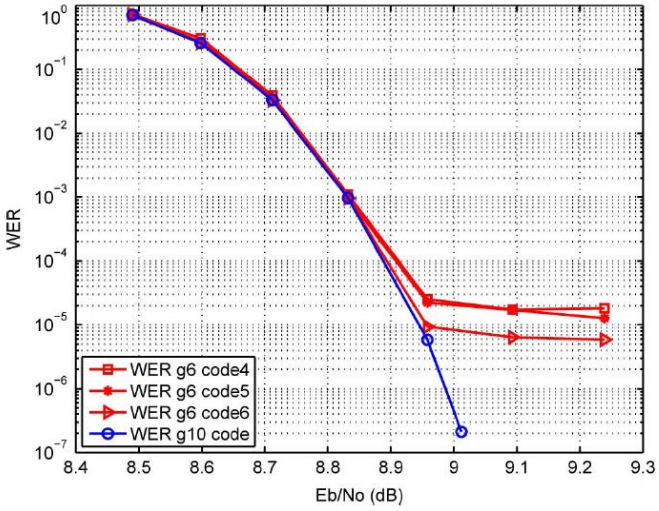

Fig. 10. Word-error rate plots of the Gallager-B algorithm for the rate-1/3, length-24000 girth-6 and girth-10 QC LDPC codes over the BSC.

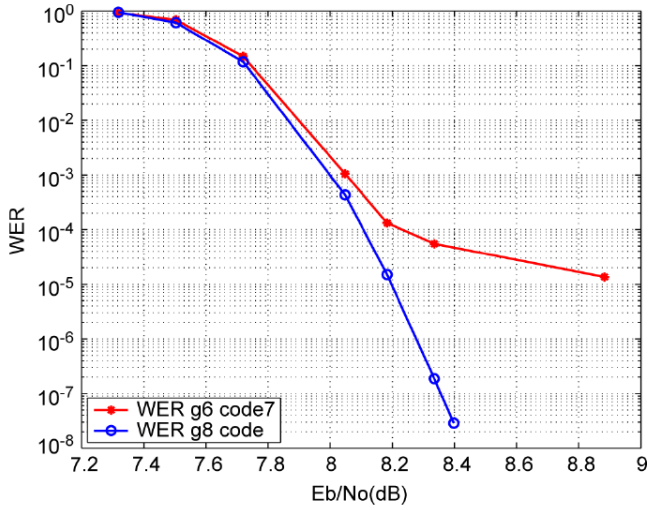

Fig. 11. Word-error rate plots of the Gallager-B algorithm for the rate-0.7, length-28000 girth-6 and girth-8 QC LDPC codes over the BSC.

- High girth or High rate → Low error floor

Ultra-Wideband Compressed Sensing : Channel Estimation

Authors: Jose L. Paredes, Member, IEEE, Gonzalo R. Arce, Fellow, IEEE, and Zhongmin Wang.
Publication: IEEE Journal of Selected Topics in Signal Processing, Octovber 2007
Speaker: Ju-Sung Kang

Short summary:

In this paper, they have introduced two novel ultra-wideband (UWB) channel estimation approaches based on compressive sensing (CS).

The proposed approach relies on the fact that transmitting an ultra-short pulse through a multipath UWB channel leads to a received UWB signal that can be approximated by a linear combination of a few atoms from a pre-defined dictionary which means sparse representation of the received signal.

The key in the proposed approach is in the design of a dictionary of parameterized waveforms (atoms) that closely matches the information-carrying pulse shape leading thus to higher energy compaction and sparse representation, and, therefore higher probability for CS reconstruction.

In the first approach, the CS reconstruction capabilities are exploited to recover the composite pulse-multipath channel from a reduced set of random projections. This reconstructed signal is subsequently used as a referent template in a correlator-based detector.

In the second approach, from a set of random projections of the received pilot signal, the Matching Pursuit algorithm is used to identify the strongest atoms in the projected signal that are related to the strongest propagation paths that composite the multipath UWB channel.

I. INTRODUCTION

1. Ultra-wideband (UWB) communications

- High bandwidth, lower-power consumption, shared spectrum resources, ranging from short-distance high-data-rate application to long-distance low-data-rate application.

- An ultra-short duration pulse is used as the elementary pulse-shaping to carry information → simplicity in the transmitter (carry-less signal), little impact on other narrowband radio system, rich in multipath diversity.

- Interference cancellation, antenna design, timing synchronization, and channel estimation. → requirement of high-speed ADC converters. : Such formiable sampling rates are not feasible with state of the art ADC technology.

- This paper focuses on this goal by casting the problem of USB channel estimation and detection into the emerging framework of CS.

2. Compressed sensing

- The remarkable result of CS reveals that with high probability, a signal, f, with a large number of data points that is M-sparse in some dictionary Ψ of basis functions, can be exactly reconstructed using only a few number of random projections of the signal onto a random basis Φ that is incoherent with Ψ.

- The number of projections is much smaller than the number of samples in the original signal leading to a reduced sampling rate and to a reduced use of ADCs resources.

3. Basic assumption

- When the short duration pulses propagate through multipath channels, the received signals remain sparse in some domain and thus CS is applicable.

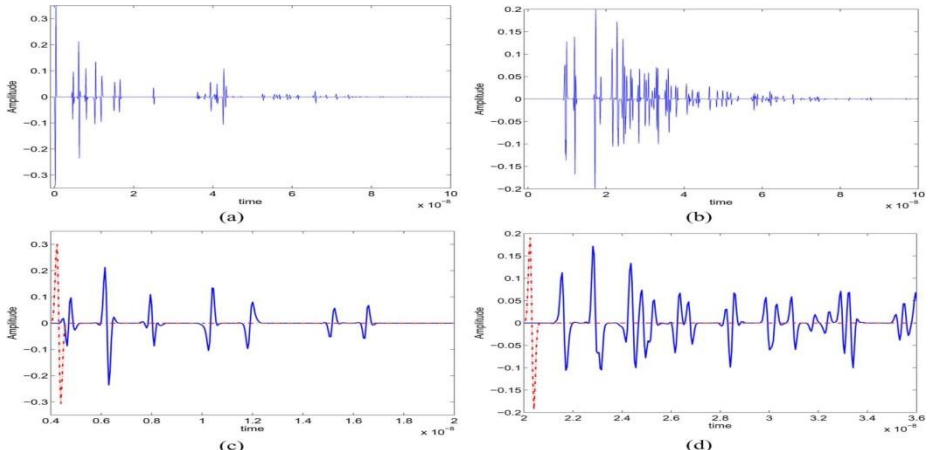

Fig. 1. Effect of UWB channel (indoor propagation in residential environments) on the transmitted pulse for two different propagation scenarios; (a) line-of-sight (LOS); (b) non-line-of-sight (NLOS); (c) zoom-in of (a); and (d) zoom-in of (b). Transmitted pulse (–.–) is also shown in (c) and (d).

- Gaussian monocycle($0.65\,\text{ns}$), IEEE 802.15.4a channel model 1 and 2(CM1, CM2).

- As depicted in above figure, the received UWB signal is composed of set of spaced clusters of the transmitted pulse which captures the statistical characteristics of multipath arivals in a UWB channel.

- It can be seen relatively long time intervals between clusters and rays where the signal takes on zero or negligible values. It is precisely this signal sparsity of the received UWB signals that is exploited in this work.

II. Ultra-Wideband Compressive Sensing.

- The sparsity of the signal can be in any domain and the number of random measurements is much smaller than the number of samples in the original signal leading to a reduced sampling rate and reduced use of ADCs resources.

1. Compressive sensing overview.

- f : N-point discrete-time representation of signal.
- y : a set of K measurements $y = \Phi f$
- Φ : $K \times N$ measurement matrix, rows are basis vectors of the space R^N
- If f is sparse, f can be written as a superposition of a small number of vector taken from a dictionary $\Psi = [\psi_1, ..., \psi_Z]$ of basis

$$f = \sum_{i=1}^{M} \theta_{l_i} \psi_{l_i} = \Psi\Theta \quad (1)$$

- $K << N$, and measurement matrix Φ is incoherent with the dictionary Ψ.
- $\Theta = [\theta_1, ..., \theta_Z]^T$ is a vector that contains M nonzeros coefficients where Z is the number of elements (atoms) in the dictionary Ψ.

- The signal f can be recovered from the solution of convex, nonquadratic optimization problem known as basis pursuit.

- But solving the optimization problem is computationally expensive and is not suitable for real-time application. So, there are more efficient recovery algorithms such as matching pursuit, orthogonal matching pursuit, and tree-based matching pursuit.

TABLE I : MATCHING PURSUIT ALGORITHM

Step A	Initialize: the residual error $e_0 = y$ the approximation $\hat{\Theta} = 0, \hat{\Theta} \in R^Z$ Interation counter $t = 1$
Step B	Select the atom in the holographic dictionary that best match the residual error. $\ell_t = \underset{i=1,2,\ldots,Z}{\arg\max} \frac{\lvert\langle e_{t-1}, v_i\rangle\rvert}{\lVert v_i \rVert}$
Step C	Update the residual error and the estimate of the coefficient for the selected vector $e_t = e_{t-1} - \frac{\langle r_{t-1}, v_{\ell_t}\rangle}{\lVert v_{\ell_t}\rVert^2} v_{\ell_t}$ $\hat{\theta}_{\ell_t} = \hat{\theta}_{\ell_t} + \frac{\langle r_{t-1}, v_{\ell_t}\rangle}{\lVert v_{\ell_t}\rVert^2}$
Step D	Check for convergence If $t < T_0$ and $\lVert e_t \rVert_2 > \epsilon \lVert y \rVert_2$ then set $t = t + 1$ and go to step B; otherwise, go to step E.
Step E	Reconstruct the signal estimate as: $\hat{f} = \Psi\hat{\Theta}$.

- MP is a computationally simple iterative greedy algorithm that tries to recover the signal by finding(in the measurement signal) the strongest component (atom of dictionary), removing it from the signal, and searching again the dictionary for the strongest atom that is presented in the residual signal.

- This procedure is iteratively repeated until the residual signal contains just insignificant information.

- Signal reconstruction is then achieved by linearly combining the set of atoms found in the measurements.

- $V = \Phi\Psi = [v_1, \ldots, v_Z]$, T_0 : maximum # of algorithm iterations, ε : the minimum energy that is left in the residual error signal.

2. Processing UWB signals Using CS.

- The received UWB signal model

$$g(t) = p(t) * h(t) = \sum_{l=0}^{L-1} \alpha_l p(t - \tau_l) \quad (3)$$

- $p(t)$: transmitting pulse, $h(t)$: noiseless UWB channel.

- We call it as composite pulse-multipath channel.

- Typically, a Gaussian pulse or its derivatives are used as $p(t)$.

- $p(t) = p_n(t) e^{-\frac{t^2}{2\sigma^2}}$, $p_n(t)$ is a polynomial of degree n that depends on the order of the derivative used.

- $h(t)$ is the impulse response of the UWB channel

$$h(t) = \sum_{l=0}^{L-1} \alpha_l \delta(t - \tau_l) \quad (4)$$

- α_l : gain factor, τ_l : delay factor, L : # of propagation paths.

- In our analysis, the set of delays and gains are generated according to the models proposed by the IEEE 802.15.4a working group in [15] . But we restrict our analysis to real-valued UWB channel models where there is not pulse distortion.

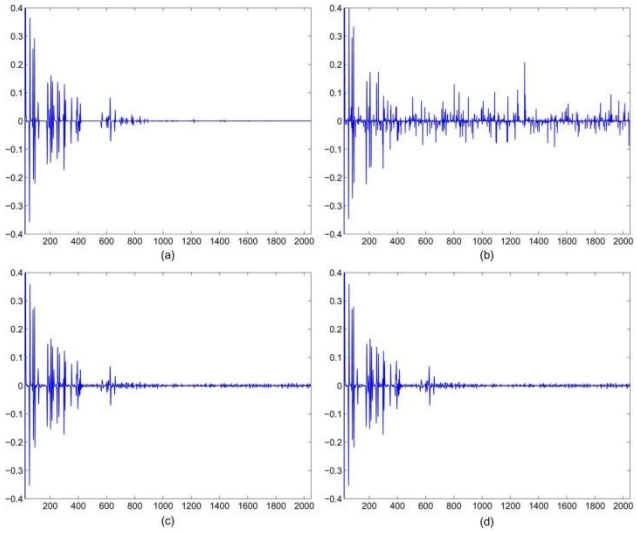

Fig. 2. (a) Received UWB signal for a realization of an indoor residential channel with LOS propagation (CM1). (b) CS reconstruction using time-sparsity model, with 500 random projections. (c) CS reconstruction using multipath diversity, with 500 random projections. (d) CS reconstruction using multipath diversity, with 250 random projections.

1) UWB signal reconstruction Using Time Sparsity Models :

- A first approach is assuming that the signal is sparse in the time domain.

- This signal model is adequate for the UWB channel in industrial environments with LOS propagation.

- $g = [g(0), g(T), ..., g((N-1)T)]^T$

- T : sampling period, N # of samples

- $\Phi \sim N(0,1)$, K*N random matrix with entries i.i.d.

- Since we are assuming sparsity in the time domain, the dictionary $\Psi = I$

- Running the MP algorithm with the $V = \Phi$ and the random projection $y = \Phi g$ yields the results show in fig.2.

- Fig. 2(a) : the 2048-point channel for a realization of an indoor residential channel with LOS propagation obtained from [15]. This is the signal targeted for reconstruction from a reduced set of random projections.

- Fig. 2(b) : the reconstructed signal obtained using 500 random measurements. Note that it fails to recover many of the signal details yielding a poor performance.

- Increasing the # of random projection means that higher sampling rate and demanding ADC resources.

- Appealing approach : to design a dictionary of parameterized waveforms where the received UWB signal can be compactly represented, increasing thus the sparsity of the underlying signal.

- This approach is motivated by the fact that the received UWB signal given by (3) can be thought of as a linear combination of the signal contributions of the various propagation paths that compose the UWB multipath channel.

2) UWB signal Reconstruction Using Multipath Diversity.

- Since CS theory relies on the fact that the underlying signal is sparse in some dictionary of basis or tight-frames, it is important to define a suitable dictionary to represent the underlying UWB signal.

- Alternatively, we can generate a new dictionary just inspecting the characteristic of the received UWB waveform.

- Since the received UWB signal is formed by scaled and delayed versions of the transmitted pulse and since the dictionary should contain elements (atoms) that can fully represent the signal of interest, it is natural to think that the elementary function to generate the atoms of the dictionary should be closely related to the pulse waveform used to covey information, i.e., the Gaussian pulse or its derivatives.

- Therefore, the dictionary is generated by shifting with minimum step Δ the generating function, $p(t)$, leading to a set of parameterized waveforms given by

$$d_j(t) = p(t - j\Delta) = p_n(t - j\Delta)e^{-\frac{(t-j\Delta)^2}{2\sigma^2}} \qquad j = 0,1,2,... \quad (5)$$

- Dictionary $D = \{d_0(t), d_1(t), ...\}$: delayed versions of the UWB transmitted pulse.

- The other definitions are same with Time Sparsity Model cases.

- $g = [g(0), g(T), ..., g((N-1)T)]^T$, T : sampling period, N # of samples, $\Phi \sim N(0,1)$, K*N random matrix with entries i.i.d.

- The MP algorithm is then applied on the random projected signal, y, and the dictionary Ψ

- Ψ is the discrete time dictionary defined by uniformly sampling the atoms of the dictionary D.

- Fig. 2(c) and (d) show the reconstructed signal using 500 and 250 random measurements, respectively. As it can be seen from Fig. 2(c) and (d), CS successfully recovers the desired signal from random projections

- Furthermore, comparing Fig. 2(b) and (c), it can be seen that reconstruction using multipath diversity outperforms reconstruction using time sparsity model

- Therefore, by building a dictionary that is closely matched to the underlying waveform, a notable performance gain is achieved in the reconstruction

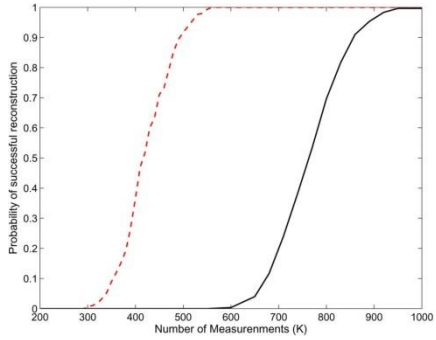

Fig. 3. Probability of success reconstruction for UWB signal for two different propagation scenarios: LOS - - - and NLOS —.

3. UWB Channel Estimation Using CS

- Consider the composite pulse-multipath channel, given by (3), where the channel parameters $\{\alpha_i, \tau_i\}_{i=1}^{L}$ related to the various propagation paths have to be estimated.

- The number of multipath components in (4) that form the UWB channel can be quite large, leading to a large time dispersion of the transmitted pulse [3].

- But only some paths have the amount of original energy. (e.g. 1160 $\rightarrow$ 70) Therefore, we limit ourselves to estimate the L_c most significant paths that composes the UWB channel impulse response

- Furthermore, the reconstruction step in the MP algorithm can be thought of as a weighted sum of the elements in the dictionary, that is $\sum_{i=1}^{Z} \theta_i d_i(t)$.

- Since each element in the dictionary is a shifted version of the transmitted pulse, it turns out that θ_i is an estimate of the path gain related to the i th propagation path.

- Furthermore, the path delay is directly determined by observing the time-location of the i th atom found in the received UWB signal.

- Let $\Theta = [\theta_1, \theta_2, ..., \theta_Z]^T$ and let let $\theta_{(k)}$ for $k = 1, 2, ..., Z$ be sorted elements of the set $\{|\theta_1|, ..., |\theta_Z|\}$. Also let $l_{(k)}$ be the index in the sparse vector of the kth sorted element. For $i = 1, 2, ..., L_C$:

$$\hat{\alpha}_i = \theta_{l_{(i)}}$$
$$\hat{\tau}_i = l_{(i)}\Delta \quad (6)$$

III. Ultrawideband Detection Based on Compressive Sensing

- Until now, we have the assumption of noiseless conditions. But we have to consider the noise and interferences.

1. UWB Signal Models.

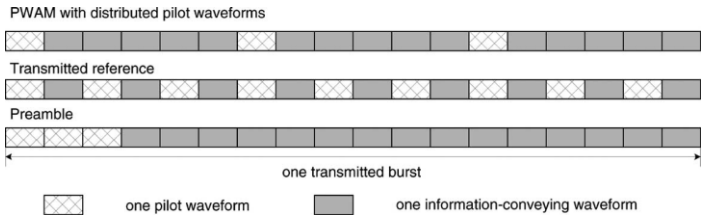

Figure. Placement of pilot waveforms for PWAM, TR, and preamble ($N_f = 3$, $N_p = 3$, $N = 18$).

- Consider a peer-to-peer UWB communication system where the k th binary information symbol is transmitted by sending N_f ultra-short pulses in the symbol interval T_s, that is [22]

$$s(t) = \sum_k b(k) \sum_{j=0}^{N_f - 1} p(t - jT_f - kT_s) \quad (7)$$

- $T_f = T_s / N_f$: frame time ; time interval between two consecutive pulses.

- $b(k) \in \{-1,1\}$: binary information symbol that modulated the amplitude of the pulse stream.

- T_p : pulse duration ; $T_p << T_f$.

- N_f nonoverlapped pulses are transmitted for each information symbol.

- The channel is static during a burst of N_s consecutive symbols. ($h(t)$ is fixed during the burst of N_s symbols).

- Let $T_f \geq \tau_{L-1} + T_p$: there is no inperpulse interference. τ_{L-1} : max delay spread of multi path channel.

- The received waveform during the first frame of the kth transmitted information symbol

$$r_f(t) = b(k) \sum_{l=0}^{L-1} \alpha_l p(t - kT_s - \tau_l) + \eta(t) \quad (8)$$

- $\eta(t)$: zero mean AWGN that models thermal noise and other interference like multi user interference.

- Since $T_f \geq \tau_{L-1} + T_p$ and the UWB channel is fixed, the received signal during the kth information symbol can be represented by periodically repeating the noiseless part of $r_f(t)$ every T_s seconds.

$$r(t) = \sum_{j=0}^{N_f - 1} r_f(t - jT_f) + \eta(t) \quad (9)$$

- Two common approaches in detection problem : correlator based detector and Rake receiver.

- In the UWB correlator-based detector, it is assumed that the channel impulse response is completely known at the receiver to define the reference template that is used in the demodulation stage.

- Likewise, for the RAKE-based receiver the channel taps $\{\alpha_{l_i}, \tau_{l_i}\}|_{i=1}^{L_r}$ related to the most significant propagation paths are assumed to be known a priori to define the set of templates for the bank of correlators and the weights for MRC [28].

- In either case, the need for UWB channel estimation arises.

- The problem of UWB channel estimation using CS under the data-aided framework. : We use N_p known pilots symbols in each packet to estimate the channel impulse response. Based on these pilots, the channel is estimated either by CS template reconstruction (Section II-B2) or CS

channel tap estimation (Section II-C). The remaining $(N_s - N_p)$ symbols that convey information are decoded based on the acquired channel characteristics.

- Under this setting, the received UWB signal (9) can be conveniently rewritten as shown in (10)

$$r(t) = \begin{cases} \sum_{k=0}^{N_w-1} b_p\left(\left\lfloor \frac{k}{N_f} \right\rfloor\right) \sum_{l=1}^{L} \alpha_l p(t - kT_f - \tau_l) + \eta(t) & for\ 0 < t < T_w \\ \sum_{k=N_w}^{(N-N_p)N_f-1} b_i\left(\left\lfloor \frac{k}{N_f} \right\rfloor\right) \sum_{l=1}^{L} \alpha_l p(t - kT_f - T_w - \tau_l) + \eta(t) & for\ T_w < t < N_s N_f T_w \end{cases} \quad (10)$$

- $N_w = N_p N_f$, T_w : time turation of the pilot waveforms.

- The received UWB signal is observed over nonoverlapped time intervals $kT_f \le t < (k+1)T_f$ for $k = 0,1,...,N_w - 1$. the received pilot waveform in a frame time is :

$$r(t) = b_p\left(\left\lfloor \frac{k}{N_f} \right\rfloor\right) \sum_{l=1}^{L} \alpha_l p(t - kT_f - \tau_l) + \eta(t) \quad (11)$$

2. CS correlator based detertor

- A first approach exploits the CS reconstruction is a correlator-based detector.

- By observing the received UWB signal in a frame-long interval and random projecting the observed signal, a noisy template can be recovered using MP algorithm. Since N_w pilot waveforms are used for channel estimation, the estimate composite pulse-multipath channel is formed by averaging over N_w noisy templates. This approach is computationally demanding as a noisy template is recovered for each received pilot waveform.

- Alternatively, the random projected signals corresponding to the received pilot waveforms can be averaged and input to the MP algorithm for template reconstruction. This latter approach requires less computation since the MP algorithm is performed just once. Furthermore, by ensemble averaging the random projected signals, the effect of AWG noise is mitigated.

- Thus, CS template reconstruction is achieved by random projecting the frame-long received signals, ensemble averaging the random projected signals, and using MP algorithm to recover an estimate of the composite pulse-multipath channel.

- Once the template has been estimated, it can be used as correlator template to enable integrate-and-dump demodulation at frame-rate sampling.

- Since each symbol is present in N_f frames, the decision statistics for the kth symbol is formed by adding up the N_f correlator output samples related to the transmitted symbol.

$$z(k) = \sum_{j=0}^{N_f-1} \int_{jT_f+kT_s}^{(j+1)T_f+kT_s} r(t) g_{cs}(t - jT_f - kT_s) dt \quad (12)$$

- $g_{cs}(t)$ is the CS estimate of the composite pulse-multipath channel.

- It can be extended to symbol-rate directly.

3. CS rake receiver

- Rake-based detectors relies on the assumption that the UWB channel parameters, path delays and path gains, related to the most significant propagation paths are known at the receiver [4], [21].

- Consider the received pilot waveform given by (11) for $k = 1, 2, ..., N_w$, where α_l and τ_l are the UWB channel taps to be estimated.

- To reduce the effect of AWGN on the estimation of the UWB channel parameters, the CS projected pilot signals are averaged to obtain a reduced-noise projected signal that is used in the MP algorithm to estimate the channel parameters as described in Section II-C.

- Thus, CS channel estimation is performed using the ensemble average of the random projections leading to a reduced computational cost and minimizing the noise effect.

- After the estimation of parameters, the CS Rake Receiver is followed.

- Let $\{\hat{\alpha}_l, \hat{\tau}_l\}|_{l=1}^{L_c}$ be the channel parameters related to the strongest paths obtained using CS channel estimation.

- The received signal, $r(t)$, is fed to a bank of L_c correlators with templates given by the atoms $p(t - \hat{\tau}_l)$ for $l = 1, 2, ..., L_c$.

- The outputs of these correlators contain the energy captured by the strongest paths and are combined via maximum ratio combining (MRC) [29] to obtain sufficient statistic for detecting the kth bit transmitted during the jth frame.

$$z_R(k,j)=\sum_{l=1}^{L_c}\hat{\alpha}_l\int_{kT_s+jT_f+\hat{\tau}_l}^{kT_s+jT_f+\hat{\tau}_l+T_p} r(t)\,p(t-kT_s-jT_f-\hat{\tau}_l)dt \quad (13)$$

- Recalling that N_f pulses are used to transmit an information symbol, the decision statistic for symbol detection is formed by summing up the MRC outputs for N_f consecutive frames.

$$\hat{b}(k)=\mathrm{sgn}\left(\sum_{j=0}^{N_f-1} z_R(k,j)\right) \quad (14)$$

IV. Simulation Results

- The Proposed CS-based detectors are compared to that of correlator detectors used in [16], [22]. : $\tilde{g}(t)=\frac{1}{N_w}\sum_{k=0}^{N_w-1} r_k(t)$ and tradition correlator (i.e. analog-template estimation followed by correlator based detector.).

- $N=10000$ symbols are transmitted.

1. BER Performance for Different Propagation Scenarios :

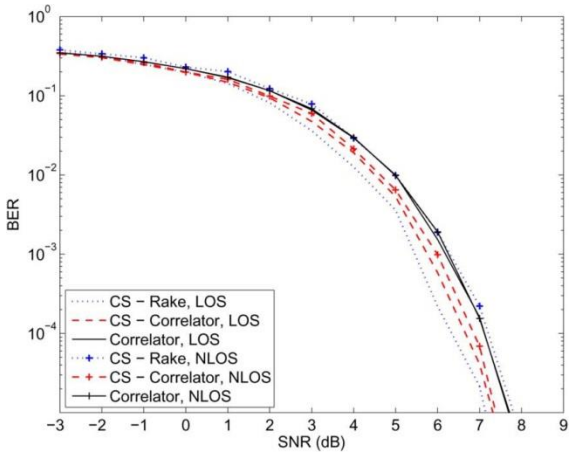

Fig. 4. Indoor residential BER performance for CS-Correlator, CS-Rake, and traditional correlator with $K/N=0.36$.

- The CS-Correlator outperforms the traditional correlator for all range of SNR.

- This shows that the reconstructed template using CS framework, $g_{cs}(t)$, is more reliable for symbol detection than the one obtained by averaging the received pilot signal, $\tilde{g}(t)$.

- This performance is expected since a denoising operation is inherently applied on the recovered signal yielding a template that is a linear combination of the transmitted pulses.

- The performance of CS-correlator for LOS channel is better than that for NLOS channel.

- This is also expected since NLOS channel introduces more multipath components than LOS channel, yielding thus a received UWB signal with less sparsity.

- CS-Rake outperforms the correlator-based detectors for LOS channel and yields competitive performance to that yielded by the traditional correlator for NLOS channel.

- As can be seen, CS-Rake degrades its performance for dense multipath channel since the CS channel estimation is unable to resolve the strongest paths among the multiple closely spaced propagation paths.

2. BER Performance for Different Number of Pilot Symbols :

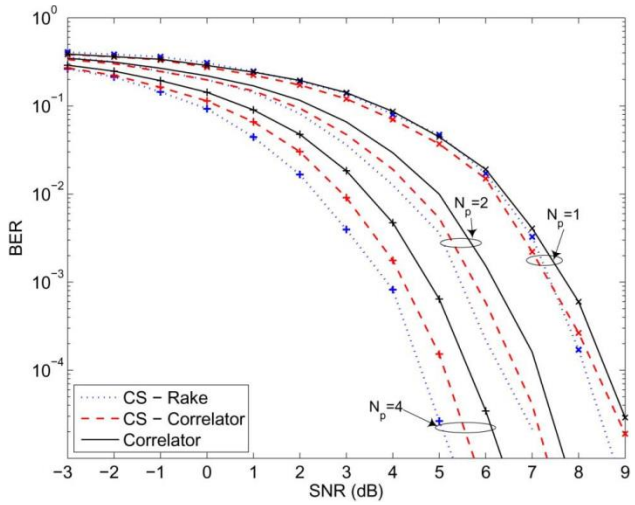

Fig. 5. BER performance for different number of pilot symbols, with $K/N = 0.36$

- Increasing the number of pilot waveforms, improvement in the channel estimation is achieved, leading to a performance gain on all the methods.

3. BER Performance for Different Number of Projections :

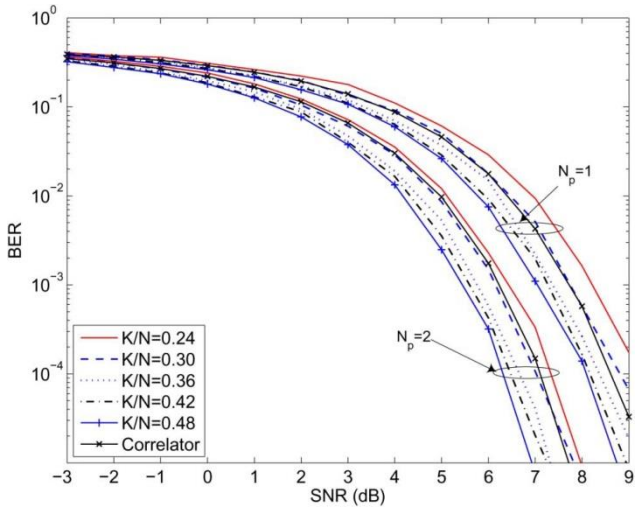

Fig. 6. BER performance for different number of projections.

- As expected, the CS-correlator's performance improves as the number of projections increases.

- More interestingly, by sampling the random projected signal at 30% of the signal's sampling rate, the CS-Correlator achieves the same performance as that yielded by the traditional correlator.

- Thus, with reduced ADC resources, the CS framework is able to reconstruct a template as good as the one obtained sampling the received UWB signal at a much higher sampling rate.

V. DISCUSSION

- What is the relation between estimated parameters and CS?

→Because of the UWB property, and the equation (3) we can use the result of MP for estimate the parameters.

- What is the value of dictionary? (form time domain to discrete domain)

→ From the uniformly sampled D, we can generate the dictionary Ψ as shifted version of pulse signal.

- How to reduce the # of samples?

→ If we think about one frame, in tradition method, we need all sample point of frame (e.g. 2048) but, by using CS, form only 250 samples, we can reconstruct the original signals.